HHS Public Access

Author manuscript

J Sound Vib. Author manuscript; available in PMC 2015 November 23.

Published in final edited form as:

J Sound Vib. 2013 February ; 232(4): 1125–1140.

Modeling of the biodynamic responses distributed at the fingers and palm of the hand in three orthogonal directions

Ren G. Dong[*], **Daniel E. Welcome**, **Thomas W. McDowell**, and **John Z. Wu**

Engineering & Control Technology Branch, National Institute for Occupational Safety and Health Morgantown, WV 26505, USA

Abstract

The objectives of this study were to develop models of the hand–arm system in the three orthogonal directions (x_h, y_h, and z_h) and to enhance the understanding of the hand vibration dynamics. A four-degrees-of-freedom (DOF) model and 5-DOF model were used in the simulation for each direction. The driving-point mechanical impedances distributed at the fingers and palm of the hand reported in a previous study were used to determine the parameters of the models. The 5-DOF models were generally superior to the 4-DOF models for the simulation. Hence, as examples of applications, the 5-DOF models were used to predict the transmissibility of a vibration-reducing glove and the vibration transmissibility on the major substructures of the hand-arm system. The model-predicted results were also compared with the experimental data reported in two other recent studies. Some reasonable agreements were observed in the comparisons, which provided some validation of the developed models. This study concluded that the 5-DOF models are acceptable for helping to design and analyze vibrating tools and anti-vibration devices. This study also confirmed that the 5-DOF model in the z_h direction is acceptable for a coarse estimation of the biodynamic responses distributed throughout the major substructures of the hand–arm system. Some interesting phenomena observed in the experimental study of the biodynamic responses in the three directions were also explained in this study.

1. Introduction

The biodynamic response of the hand–arm system to vibration is an important component of the physical process leading to the development of hand–arm vibration syndrome [1,2]; hence, further study of it may enhance the understanding of the mechanisms of the syndrome and help in developing more effective methods for quantifying vibration exposures to establish a more reliable dose–response relationship between the exposure and the major vibration effects. A recent study hypothesized that the frequency-dependency of a vibration effect can be factored into biodynamic frequency weighting and biological frequency weighting [3]. The biodynamic frequency weighting may play a dominant role in determining the frequency-dependencies of some vibration effects. For example, it has been

[*] Corresponding author. Tel.: +1 304 285 6332; fax: +1 304 285 6265. rkd6@cdc.gov (R.G. Dong)..

Disclaimers

The content of this publication does not necessarily reflect the views or policies of the National Institute for Occupational Safety and Health (NIOSH) nor does mention of trade names, commercial products, or organizations imply endorsement by the US Government.

demonstrated that the frequency-dependency of the vibration power absorption of the hand–arm system [4], as a measure of the overall biodynamic response, is similar to the current frequency weighting for assessing the risk of the hand-transmitted vibration exposure [5], which was determined primarily based on the sensation contours of the entire hand–arm system [6]. It has also been further hypothesized that the biodynamic response within a substructure of the hand–arm system may be more closely associated with the local effects or disorders within that substructure than the overall response of the system [2,3]. While this has been demonstrated in a previous study [7], further tests of these hypotheses require developing more effective methods for quantifying the distributed biodynamic responses. Although many studies have examined the biodynamic response of the entire hand–arm system [8–14], and the International Organization for Standardization (ISO) has set forth a standard on the overall biodynamic response function [15], the distributed or substructure-specific responses have been far from sufficiently studied.

While no *in vivo* method has been developed to directly measure the distributed responses inside the substructures of the hand–arm system, their quantifications have been primarily based on modeling of the system [5,16]. Many models of the hand–arm system have been proposed, and the vast majority of them can be found in some reviews [17,18]. Probably because a single-point hand-handle coupling has been traditionally assumed in the experimental studies of the vibration biodynamic responses of the hand–arm system, the hand has been considered as an entity or mass coupled to a handle at a single point in most of the reported models. These models cannot be applied to simulate the biodynamic responses distributed at the fingers and palm, which may be very important for the further study of hand-transmitted vibration exposures and related health effects. Although some of these mechanical-equivalent models may have an excellent fit to the measured driving-point response functions and may be acceptable for the designs and analyses of some tools and anti-vibration devices [19], it is difficult to establish the relationship between a specific component of the models and a specific substructure of the hand–arm system. This also makes it very difficult to apply these models to predict the responses distributed in the various substructures of the hand–arm system.

The finite element (FE) method may be the best available technique for modeling the detailed biodynamic responses distributed inside the system. Some FE models of local structures have been developed and applied in studies [7–16]. However, the development of a sufficiently validated FE model of the entire hand–arm system remains a formidable research task. FE modeling is also usually expensive and time-consuming. For a crude estimation of the distributed responses, a lumped-parameter model of the system may be acceptable for some applications. The above-mentioned deficiencies of the single-point hand coupling models have also been partially overcome by using a two-point coupling approach initially proposed by Dong et al. [20]. This approach divides the hand contact area into two parts: one at the fingers and the other at the palm of the hand. While a reliable method has been developed to measure the biodynamic responses distributed at these two locations [21], two lumped-parameter models of the hand–arm system have been proposed to simulate the distributed responses [22]. One of the models was applied to estimate the vibration power absorptions distributed among the major substructures of the system [23]. This model also

provided a reasonable estimation of the vibration transmissibility of a vibration-reducing glove [24]. These two-point coupling models have been adopted in a proposed revision of ISO 10068 [25]. In a recent study, the two-point hand coupling models were expanded to include more degrees of freedom so that the models could predict more detailed responses distributed in the arm–shoulder substructures [26]. These observations suggest that this efficient modeling approach still has some value for further studies and applications.

The models established based on the two-point hand coupling approach were primarily used for studying the distributed responses along the forearm direction (z_h) of the system [22–24,26]. Only one experimental study reported the biodynamic responses distributed at the fingers and palm of the hand in the directions (x_h and y_h) orthogonal to the forearm direction [27]. It was unclear whether the models for the z_h direction could also fit these experimental data because they exhibit some large differences. However, for completeness and consistency, the two-point coupling models in these two directions have also been included in the proposed revision of the ISO standard [25]. These models were established based on the responses of the entire hand–arm system recommended in the original standard [15]. It was unclear how to interpret their model parameters and whether the adopted models are actually acceptable for simulating the distributed responses. Furthermore, as implied in a recent study [26], the validity of the model established based on the driving-point biodynamic response function in the z_h direction also needs further examination.

This study hypothesized that it is acceptable for simulating the driving-point biodynamic response functions directly measured at the fingers and palm of the hand using the original two-point coupling models not only in the z_h direction but also in the other two directions, and they are thus acceptable for some applications. This study also hypothesized that the two-point models could help explain some phenomena observed in the experimental study of the 3-D biodynamic responses [27]. Therefore, the specific aims of this study are to create two-point-coupled models in the three orthogonal directions based on the distributed mechanical impedances and to enhance the understanding of the 3-D vibration biodynamics of the hand. As examples of applications, one of the developed models was used to predict the vibration transmissibility on several hand–arm substructures and the transmissibility of a vibration-reducing glove. The model-predicted transfer functions were compared with some reported experimental data. The implications of the modeling results and comparisons are discussed.

2. Methods

The driving-point biodynamic response functions such as apparent mass and mechanical impedance of the hand–arm system are measures of the overall biodynamic properties of the system; hence, the response function can be used to calibrate a given model of the system or to determine its parameters. Because apparent mass generally decreases with the increase in frequency, a model established based on apparent mass emphasizes the low-frequency response components. Impedance (Z) is related to apparent mass (M_A) as follows [1]: $Z = j\omega \cdot M_A$, in which ω is the angular frequency and $j = \sqrt{-1}$. A model calibrated using impedance generally highlights the resonance frequency regions of the system because the impedance has a relatively large value in such regions. Also importantly, the impedance is directly

associated with the vibration power absorption. Therefore, models of the hand–arm system have been more frequently established based on mechanical impedance [17,18]. This method was thus adopted in this study.

2.1. Experimental data

The experimental data used in this study were reported in a previous study [27]. In that study, seven subjects participated in the measurements of the driving-point mechanical impedance distributed at the fingers and the palm of the hand exposed to three-dimensional vibrations. A broadband random vibration in the 16–500 Hz range was used as the excitation in each direction. As shown in Figs. 1 and 2, each subject was instructed to stand upright on a force plate for push force measurement and to grasp an instrumented handle for the vibration and grip force measurements. The elbow angle was controlled to remain between approximately 90° and 120°; the elbow was not in contact with the body during the measurements. The applied hand forces were 30 N grip and 50 N push. These subject postures and hand forces are similar to those required in the standardized anti-vibration glove test [28] and for the mean impedance data recommended in the current ISO 10068 [15] and its proposed revision [25]. The measured biodynamic force and acceleration data were analyzed to derive finger and palm-side mechanical impedance values, expressed in the one-third octave bands with center frequencies from 16 Hz to 500 Hz. In the experiment, the 3-D vibration transmissibility was also measured at several locations on the surfaces of the hand–arm system using a 3-D laser vibrometer [29]. The transmissibility data were also compared with those predicted with the models developed in the current study.

2.2. Model configurations

Fig. 3 shows the configurations of the two models for the z_h direction [22]. In terms of the number of mass elements in the models, they are referred to as 5-DOF and 4-DOF models, respectively. The hand holding a vibrating cylindrical handle is simulated using a clamp-like mechanical system that virtually divides the hand into two parts about the centerline of the handle. The upper portions of the diagrams represent the fingers positioned on one side of the handle, and are simulated using two masses (M_4 and M_2) coupled via linear stiffness (K_4) and viscous damping (C_4). M_4 represents the effective mass of finger skin contacting the handle whereas M_2 is the effective mass due to the remaining finger tissues, mainly composed of finger bone masses. The lower portions of the diagrams constitute the palm–wrist–forearm substructures represented by two masses (M_3 and M_1) coupled via K_3 and C_3. Whereas M_3 represents the effective mass of palm skin contacting the handle, M_1 represents the remaining effective mass of the palm–wrist–forearm substructures; because the wrist joint is very stiff along the forearm direction, the masses of the remaining palm–wrist–forearm substructures are lumped together. While the effective mass of the elbow–upper arm–shoulder substructures is not considered in the 4-DOF model, it is represented by M_0 in the 5-DOF model. A group of spring–damper elements (K_1 and C_1 in the 4-DOF and K_0 and C_0 in the 5-DOF) was used to represent the boundary condition of each model.

As shown in Fig. 4, the model structures for the x_h and y_h directions are exactly the same as those for the z_h direction. While simulations of the fingers in the x_h and y_h directions are the same as those for the z_h direction, the elements in the lower portions of the model diagrams

in Fig. 4 require some differences in their physical interpretations. Because the wrist is flexible in the x_h and y_h directions, flexible connectors are required to link the effective masses of the palm and hand dorsum to that of the forearm in the models for those axes. Therefore, M_1 in these models represents only the effective mass of the palm–hand dorsum substructure. Then, the effective mass of the wrist and forearm is represented by M_0 in the 5-DOF model, and this mass is not reflected in the 4-DOF model. The effective mass of the elbow–upper arm–shoulder substructures could not be considered in the 5-DOF model in either the x_h or y_h direction.

2.3. Calculation of the driving-point mechanical impedances

The equations of motion for each model subjected to handle excitation are expressed in the matrix form as

$$\mathrm{M}\ddot{\mathrm{q}}+\mathrm{C}\dot{\mathrm{q}}+\mathrm{Kq}=\mathrm{F}, \quad (1)$$

where **M** is the mass matrix, **C** is the damping matrix, **K** is the stiffness matrix, **F** is the force vector and **q** represents the vector response coordinates in x_h, y_h, or z_h direction.

The same approach described in the previous studies [22,23] was used to resolve the equations and to compute the driving-point mechanical impedance. Briefly, the equations of motion for each direction were solved separately by assuming a given excitation from the handle at each frequency. The vibration forces acting at the fingers and palm were calculated from the obtained relative displacements at the interfaces. Then, the driving-point mechanical impedance was calculated for each direction for the finger side (Z_{Fingers}) and for the palm side (Z_{Palm}).

2.4. Model constraints

In addition to the reliability of the experimental data, the computational effectiveness and validity of the optimized results largely depend on reasonable constraints of the model parameters. While it is difficult to determine the exact ranges for the stiffness and damping parameters in the models, a refined range for each modeled mass element can be estimated based on the enhanced representation of each substructure within the models.

Based on the above-described model configurations and the results of studies reported before [22,23], the constraints for the models in the z_h direction were as follows:

$$\begin{gathered} 1000 \leq K_0, K_1, K_2, K_3, K_4 \leq 160,000\mathrm{N/m} \\ 5 \leq C_0, C_1, C_2, C_3, C_4 < 300\mathrm{Ns/m} \\ 4.0 < M_0 \leq 6kg\,(\text{upper arm and shoulder}) \\ 0.5 < M_1 \leq 2kg\,(\text{palm, wrist, and forearm}) \\ 0.05 < M_2 \leq 0.12kg\,(\text{finger bones and part of the finger soft tissues}) \\ 0.001 < M_3 < 0.040kg\,(\text{palm contact skin}) \\ 0.001 < M_4 < 0.030kg\,(\text{finger contact skin}) \end{gathered} \quad (2)$$

Whereas the contact stiffness and damping parameters of the fingers may vary greatly with direction, their effective mass contributions should be very similar in each direction because the actual finger mass is not a function of vibration direction. The reported studies indicate that the modeled finger effective mass in the z_h direction (M_{2_zh}) can be distinctly determined [22,23]. However, the preliminary simulations performed in the current study indicated that the values for the finger effective mass (M_2) in the x_h and y_h direction models could depend on the initial conditions. Therefore, the constraints of M_2 in the x_h and y_h directions were based on those identified from the simulation in the z_h direction. The preliminary trials also revealed that the model outputs for these two directions could not fit well with the experimental data without greatly reducing the lower boundary of K_2. Because M_0 and M_1 represent different substructures from those in the z_h direction models, their constraints in the x_h and y_h directions were also different. The revised constraints for these two directions are summarized as follows:

$$\begin{gathered} 0.3 \leq M_0 \leq 2.0kg\,(\text{rotational- equivalent mass of forearm}) \\ 0.1 \leq M_1 \leq 0.50kg\,(\text{palm and hand dorsum}) \\ 0.95M_{2\_zh} \leq M_2 \leq 1.05M_{2\_zh}\,(\text{finger mass}) \\ 10 \leq K_2 \leq 10,000\text{N/m}. \end{gathered} \tag{3}$$

2.5. Procedures for determining the model parameters

As in the previous studies [22,23], the parameters for each model were determined based on the measured data through the solution of an optimization progression to minimize the constrained error function. First, the root-mean-square difference between the measured and model impedances was calculated from

$$\Delta Z = \sqrt{\frac{1}{N}\sum_{i=1}^{N}(Z_{Pi} - Z_{Ei})^2}, \tag{4}$$

where Z_{Pi} and Z_{Ei} are model-predicted and experimental impedance values measured at the fingers or the palm at the center frequency of the ith frequency band, respectively, and N is the number of one-third octave frequency bands considered in the analysis.

Then, a total error function E(χ), comprising the sum of deviations in Z_{Fingers} and Z_{Palm}, was calculated from

$$E(\chi) = Re\left[\Delta Z_{\text{Fingers}}(j\omega)\right] + Im\left[\Delta Z_{\text{Fingers}}(j\omega)\right] + Re\left[\Delta Z_{\text{Palm}}(j\omega)\right] + Im\left[\Delta Z_{\text{Palm}}(j\omega)\right], \tag{5}$$

where '*Re*' and '*Im*' designate the real and imaginary components of impedance, respectively, corresponding to center frequency χ; and w is the vector of model parameters, given by

$$\chi_5 - \mathrm{DOF} = [M_0, M_1, M_2, M_3, M_4, K_0, K_1, K_2, K_3, K_4, C_0, C_1, C_2, C_3, C_4] \quad (6)$$

for the 5-DOF model, or

$$\chi_{4-\mathrm{DOF}} = [M_1, M_2, M_3, M_4, K_1, K_2, K_3, K_4, C_1, C_2, C_3, C_4] \quad (7)$$

for the 4-DOF model.

For model parameter identification, each model parameter was varied sequentially until the resulting error function in Eq. (5) attained a minimum value. The process was repeated until the solutions corresponding to two consecutive iterations converged to similar error values or with their difference <0.001 N s/m. The goodness-of-fit between the modeling and experimental data was also assessed using the *R*-value of the curve fitting.

Due to the requirements of the constraints in Eq.(2), the model parameters for the models for the z_h direction were first determined using the above-described procedures. Then, the same procedures with the constraints in Eq. (3) were used to determine the model parameters for the other two directions.

3. Results

3.1. Simulated mechanical impedances

The comparisons of the measured driving-point mechanical impedances (arithmetic averages of the data measured with the seven subjects [27]) distributed at the fingers and palm of the hand with those simulated using the 5-DOF and 4-DOF models are shown in Figs. 5 and 6, respectively. The agreement between the experimental and the modeled data in each of the three directions was excellent (*R*-value ≥ 0.958) when the 5-DOF model was used, as shown in Fig. 5. The 4-DOF model also provided an excellent simulation of the responses at the fingers in each direction (*R*-value ≥ 0.956), as shown in Fig. 6. The agreements between the measured and simulated impedances at the palm in the z_h and y_h directions were also excellent (*R*-value ≥ 0.983). However, the 4-DOF model could not provide suitable simulations of both magnitude and phase angle of the impedance at the palm in the x_h direction at frequencies below 60 Hz, as shown in Fig. 6.

3.2. Mean response-based model parameters

When the model parameters were determined based on the mean impedances of the subjects, these parameters were termed as mean response-based model parameters [30]. Table 1 lists such parameters of the 5-DOF and 4-DOF models. The corresponding parameters for simulating the fingers (M_2, M_4, K_4 and C_4) in the two models for each direction were similar. These four parameters in the x_h and z_h directions were also comparable. However, except M_2, they were largely different from those in the y_h direction, especially the stiffness and damping values. Similar phenomena were observed for the simulations of palm stiffness and damping (K_3 and C_3).

As also indicated in Table 1, because M_0 and M_1 in the z_h direction represent the effective masses of additional hand-arm substructures, their values were larger than those in the x_h and y_h directions. For the same reason, there were also some differences in their related connecting stiffness and damping values (K_0, C_0, K_1 and C_1). The K_2 values in the x_h and y_h directions were much smaller than those in the z_h direction.

3.3. Mean property-based model parameters and impedances

When the model parameters were first determined based on the impedances of each subject and the averages of the parameters were used to define the general model of all the subjects, they were termed as mean property-based model parameters [30]. The comparisons of the mean property-based and mean response-based model parameters are provided in Table 2. In the vast majority of cases, the corresponding parameter values are only marginally different (< 15 percent), especially those parameters of the elements simulating the substructures close to the hand-handle contact points.

The comparisons of the mean response-based and mean property-based modeling results are shown in Fig. 7. The differences in the impedances at the fingers were generally less than 10 percent. However, some large differences (< 22 percent) were observed at the first resonance of the impedance at the palm in each direction. A study indicated that the mean property-based models are more reliable than the mean response-based models [30]; hence, the mean property-based models were used in the following applications.

3.4. Prediction of the vibration transmissibility on the hand-arm system

The vibration transmissibility functions for three mass elements (M_0, M_1, and M_2) in the mean property-based 5-DOF model in each direction were calculated. In the z_h direction, they are assumed to represent the transmissibility of the upper arm, the palm–wrist–forearm, and the fingers, respectively. These assumptions were consistent with the experimental data [29], as shown in Fig. 8. The M_0-transmissibility agreed well with that measured at a distal location on the upper arm (approximately 1/4 of the distance from the elbow joint to the shoulder); the M_1-transmissibility was surprisingly well-matched with that measured at the wrist; and the M_2-transmissibility was also comparable with the average transmissibility of those measured at ten points on the thumb, index finger, and middle finger [29].

The comparisons in the y_h direction are shown in Fig. 9. The basic trends and fundamental resonant frequencies at each of the three locations (wrist, hand dorsum, and fingers) were approximately predicted from the model. However, there were substantial differences between predicted and measured transmissibility magnitudes. As shown in Fig. 10, the comparisons in the x_h direction are similar to those in the y_h direction, except that the model in the x_h direction did not predict the same trend of transmissibility as that measured in the experiment in the important frequency range of 40–200 Hz.

3.5. Prediction of the transmissibility of a vibration-reducing glove

A previous study found that a vibration-reducing glove can be approximately simulated as a mass–spring–damper system, and the basic trend of glove transmissibility in the z_h direction can be reasonably predicted [24]. A simplified version of the glove model is incorporated in

the 5-DOF hand–arm system model and included in the proposed revision of ISO 10068 [25], which is shown in Fig. 11. This glove–hand–arm system model was also adopted to predict the transmissibility of a vibration-reducing glove in the current study. For simplicity, the mass, stiffness, and damping values for the glove modeling were assumed to be the same as those recommended in the proposed revision of the standard for each direction [25]. The parameter values are also shown in Fig. 11.

The comparisons of the model-predicted and measured transmissibility functions in the three directions are shown in Fig. 12. The experimental data were measured on a viscoelastic gel-filled vibration-reducing glove [31]. The palm transmissibility functions in the three directions were measured using a palm adapter under the same test conditions (excitation, hand and arm postures, hand forces) as those used in the measurement of the 3-D mechanical impedances [31]. As shown in Fig. 12(a) and (b), the basic characteristics of the model-predicted transmissibility in the z_h direction were comparable with those of the experimental data. This also held true for the comparisons in the y_h direction. The agreement in the x_h direction is not as strong as those in the other two directions, but the basic trends of the model-predicted and measured data are consistent in the high-frequency range critical for glove assessments [28].

The experimental data of the gel-filled glove finger transmissibility shown in Fig. 12 were measured using a 3-D laser vibrometer under the same test conditions as mentioned above [30]. The glove transmissibility at each frequency was calculated from the gloved-finger transmissibility and the bare-hand finger transmissibility [32]. Because the glove could substantially alter the finger positions and orientations relative to the handle, it was difficult to reliably determine the direction-specific transmissibility. Hence, only the total vibration (vector summation of the three axial vibrations) transmissibility was calculated in the experimental study [32]. As shown in Fig. 12(c) and (d), the basic trends of the model-predicted glove finger transmissibility are comparable with those of the experimental data. Both the modeling results and experimental data suggest that the studied glove cannot reduce finger-transmitted vibration at frequencies below 100 Hz; in fact, the glove marginally amplified the finger-transmitted vibration in this frequency range.

4. Discussion

Two models of the hand–arm system (4-DOF and 5-DOF) were developed in this study. Eliminating the skin mass elements (M_3 and M_4) in rigid contact with the handle, the 4-DOF and 5-DOF models established in this study have only two and three effective DOFs, respectively. It is impossible to use such simple models to accurately predict the responses distributed in the complex hand–arm system. However, the reasonable simulations of the mechanical impedances distributed at the fingers and palm of the hand shown in Figs. 5–7 suggest that the major overall dynamic features of the system observed at the driving point are refiected by the models, especially the 5-DOF models. Therefore, these models are useful for some applications. This study also provided some useful information for understanding the vibration dynamics of the hand.

4.1. Vibration characteristics of the hand holding a cylindrical handle

The undamped natural frequency of the fingers (f_2) in each direction listed in Tables 1 and 2 can be approximately calculated from their major effective mass (M_2) and contact stiffness (K_4). Another major resonant frequency (f_1) listed in the tables is also directly related to the palm contact stiffness (K_3). These frequencies fall into the major vibration frequency range (10–500 Hz) of the vast majority of powered hand tools [33]. These resonant frequencies are also within the dominant frequency range (25–250 Hz) of tools that are most often associated with vibration-induced white finger [1].

The results of this study indicate that the finger contact stiffness (K_4) in each vibration direction is much larger than the palm contact stiffness (K_3), as presented in Tables 1 and 2. This is primarily because the palm comprises thicker soft tissue. The values of K_3 and K_4 in the y_h direction are much less than those in the other two directions. This shows that the shear stiffness of the hand is much less than the compression stiffness. The stiffness in the x_h or z_h direction in the models actually includes both compression stiffness and shear stiffness. This suggests that the pure compression stiffness is likely to be larger than the stiffness values listed in the tables. As also indicated in Table 2, the finger contact stiffness (K_4) in the x_h direction (109 kN/m) is only about 6 percent larger than that in the z_h direction (103 kN/m). When the finger response is largely independent of the remaining hand–arm substructures at high frequencies (4 100 Hz), the similar mass and stiffness values in these two directions lead to similar impedance responses in these two directions [27]. It is also interesting to note that the palm contact stiffness (K_3) in the x_h direction (43 kN/m) is only about 16 percent larger than that in the z_h direction (36 kN/m). This explains why the impedances in these two directions are also comparable in the high-frequency range when the vibration cannot be effectively transmitted beyond the hand [27]. These observations support the hypothesis that the responses of the hand gripping a cylindrical handle in the x_h–z_h plane are similar to the direction-independent responses of a symmetrical rubber ring wrapped around the handle [6].

As shown in Fig. 5, the phase angle of the measured impedance of the fingers in the low-frequency range could be more than 90° in the x_h and y_h directions. When the angle is more than 90°, the vibration power absorption measured at the fingers is negative, which implies that more power would flow back into the handle than would flow into the fingers. This appears to be very unusual, and it may partially result from measurement errors because it is difficult to accurately measure low finger impedance in the low-frequency range with low excitation [27]. However, such a phenomenon was also replicated in this modeling study, as shown in Figs. 5–7. This suggests that such a phenomenon is physically possible, and it may not be solely attributed to measurement errors. However, the exact mechanism may not be the same as that predicted in the simulation. As shown in Table 2, this process requires a connection with very little stiffness (K_2) but relatively large damping (C_2) between the fingers and the hand dorsum in the x_h and y_h directions. Such connection conditions may not actually exist. Hence, the phenomenon may only be a mechanical-equivalent simulation in this study. The real mechanism may be related to the rotational responses of the hand dorsum–fingers substructure. Theoretically, the finger response is essentially the superposition of the response to the vibration transmitted from the handle to the fingers and

the response to the palm-transmitted vibration. The latter component may be understood by conceptually considering the dorsum–fingers substructure as a continuously supported cantilever anchored at the palm–handle interface. In the low-frequency range, when palm-transmitted vibration is the prevailing factor in the response, the bending or rotation of this cantilever-like structure may be the dominant influence on the finger response at some frequencies. Under such circumstances, the fingers may actually transmit some vibration power from the palm–dorsum–fingers back into the handle at the fingers–handle interface. This hypothesis could not be tested using the models developed in this study; its test requires including the rotational components in the modeling in further investigation.

4.2. An evaluation of the models in the proposed revision of ISO 10068

Table 3 lists the parameters of the 5-DOF models included in the proposed revision of the ISO standard [25], together with those of the property-based 5-DOF models developed in the current study. Their model-predicted responses are shown in Fig. 13. Because the models are established based on experimental data from different sources [14,34], it is normal to see some differences in the comparisons. However, the distributed response functions shown in Fig. 13(b) in the x_h and y_h directions show more differences than their corresponding total responses shown in Fig. 13(a). This might suggest that the predicted distributions using the proposed ISO models in these directions are unlikely to be representative of the actual distributions. The parameters of the models in these two directions also suggest that these models do not reasonably reflect some important features of hand biodynamics. For example, the palm contact stiffness (K_3) in the model for the x_h or y_h direction is unrealistically much lower than that in the new model, as reflected in Table 3. The finger contact stiffness (K_4) and palm contact stiffness (K_3) in the proposed ISO model in the x_h direction were also unreasonably much lower than those in the z_h direction for that model.

As also shown in Fig. 13, the resonance features reflected in the proposed ISO model in the z_h direction are similar to those shown in the new model. The better performance of the ISO model in this direction may be partially because its corresponding experimental data were updated when the standard was revised, but no new data were available at that time for updating the data in the x_h and y_h directions [34]. Furthermore, the model constraints used in the z_h direction were defined based on the available model parameters delineated using the actual distributed impedance data [22,23,34]; however, such models in the x_h and y_h directions were not available until the current study. These observations suggest that the standard can be further improved when sufficient reliable experimental data in these two directions are available and more reliable models are developed in further investigation.

4.3. Applications and major limitations of the models developed in this study

The comparisons shown in Fig. 6 suggest that the 4-DOF models are acceptable for simulating the overall responses of the fingers. It is also easier to physically build mechanical simulations or prototypes of the hand–arm system based on the 4-DOF models than the 5-DOF models. However, as shown in Fig. 5, the 5-DOF models are a better choice when the responses of the palm–wrist–forearm substructures are also of concern. The results shown in Fig. 7 further suggest that it is better to use the property-based 5-DOF models for

enhancing designs and analyses of powered hand tools and anti-vibration devices. The reasonable predications of the glove transmissibility shown in Fig. 11 also suggest these 5-DOF models are acceptable for such applications. However, it should be noted that these models were established based on the impedance data in the frequency range of 16–500 Hz. They should be used with caution beyond this frequency range. Moreover, the models were calibrated from the experimental data measured under the specific conditions described in Section 2.1. They should also be applied with caution to the cases with largely different conditions.

The reasonable agreement between the model-predicted and measured data of the vibration transmissibility shown in Fig. 8 suggests that the 5-DOF model in the z_h direction is acceptable for approximately predicting the transmissibility at some locations on the upper arm and at the wrist. It may also be used to crudely predict the finger average transmissibility. The agreement also supports the use of the model for a crude estimation of the vibration power absorption distributed in the major substructures such as the fingers, palm–wrist–forearm, and upper arm–shoulder, as was done in a previous study [23].

The hand and arm postures used to measure the transmissibility on the hand dorsum were different from those used for measuring the impedance, because the laser beams were blocked by the handle fixture (Fig. 1) with the postures for the impedance measurement [29]. This may partially explain the large differences shown in Figs. 9(b) and 10(b). Also due to fixture interference, the finger transmissibility was only measured on part of the fingers. This may also partially explain the disagreement between the model-predicted and measured finger transmissibility data shown in Figs. 8(c), 9(c) and 10(c). However, the large differences observed in the x_h and y_h directions suggest that the model structure used in this study may need some improvements to better represent the transmissibility response in these directions. Not directly accounting for the cross-axis responses and rotational responses in these models may also contribute to discrepancies. The experimental data should also be further examined. In any case, the observed large differences suggest that the models in the x_h and y_h directions should not be used to predict the transmissibility and vibration power absorption before they are further improved and validated.

5. Conclusions

This study enhanced the understanding of hand vibration biodynamics. Two sets of lumped-parameter models of the hand–arm system in three orthogonal directions, respectively with 4-DOFs and 5-DOFs, were defined based on the driving-point mechanical impedances distributed at the fingers and palm of the hand. The 5-DOF models are superior to the 4-DOF models in most simulations, and they can be used to help design and analyze powered hand tools and anti-vibration devices. The 5-DOF models also reasonably predicted the basic trends of the transmissibility of a vibration-reducing glove, which suggests that the models are acceptable for further understanding and designing such gloves. The 5-DOF model in the z_h direction also provides acceptable predictions of the vibration transmissibility at a point on the upper arm, at the wrist, and on the fingers. This suggests that the model in the z_h direction is acceptable for coarse estimations of the biodynamic responses distributed in major substructures of the hand–arm system. However, there are

some large differences between the model predictions and the experimental data for vibration transmissibility in the x_h and y_h directions. The model structures used in this study are also insufficient to predict the arm and shoulder responses in these two directions. Therefore, further studies are required to improve them.

References

[1]. Griffin, MJ. Handbook of Human Vibration. Academic Press; London: 1990.

[2]. Dong RG, Wu JZ, Welcome DE. Recent advances in biodynamics of hand–arm system. Industrial Health. 2005; 43(3):449–471. [PubMed: 16100922]

[3]. Dong. D.E. Welcome RG, McDowell TW, Xu XS, Krajnak K, Wu JZ. A proposed theory on biodynamic frequency weighting for hand-transmitted vibration exposure. Industrial Health. 2012; 50(5):412–424. [PubMed: 23060254]

[4]. Dong RG, Welcome DE, McDowell TW, Wu JZ, Schopper AW. Frequency weighting derived from power absorption of fingers–hand–arm system under z_h-axis. Journal of Biomechanics. 2006; 39:2311–2324. [PubMed: 16154576]

[5]. ISO 5349-1: Mechanical Vibration—Measurement and Evaluation of Human Exposure to Hand-Transmitted Vibration. Part 1: General Requirements. International Organization for Standardization; Geneva, Switzerland: 2001.

[6]. Miwa T. Evaluation methods for vibration effects. Part 3: measurement of threshold and equal sensation contours on hand for vertical and horizontal sinusoidal vibration. Industrial Health. 1967; 5:213–220.

[7]. Wu JZ, Krajnak K, Welcome DE, Dong RG. Analysis of the dynamic strains in a fingertip exposed to vibration: correlation to the mechanical stimuli on mechanoreceptors. Journal of Biomechanics. 2006; 39:2445–2456. [PubMed: 16168999]

[8]. Burström L. The influence of biodynamic factors on the mechanical impedance of the hand and arm. International Archives of Occupational and Environmental Health. 1997; 69(6):437–446. [PubMed: 9215931]

[9]. Kihlberg S. Biodynamic response of the hand–arm system to vibration from an impact hammer and a grinder. International Journal of Industrial Ergonomics. 1995; 16:1–8.

[10]. Kinne, J.; Latzel, K.; Schenk, TH. Application of two-hand impedance as basis for mechanical modeling. Proceedings of the Ninth International Conference on Hand–Arm Vibration; Nancy, France. 2001. p. 113-118.pp.

[11]. Marcotte P, Aldien Y, Boileau PE, Rakheja S, Boutin J. Effect of handle size and hand-handle contact force on the biodynamic response of the hand–arm system under z_h-axis vibration. Journal of Sound and Vibration. 2005; 283(3–5):1071–1091.

[12]. Aldien Y, Marcotte P, Rakheja S, Boileau P-E. Influence of hand–arm posture on biodynamic response of the human hand–arm exposed to z_h-axis vibration. International Journal of Industrial Ergonomics. 2006; 36:45–59.

[13]. Besa AJ, Valero FJ, Suñer JL, Carballeira J. Characterisation of the mechanical impedance of the human hand–arm system: the influence of vibration direction, hand–arm posture and muscle tension. International Journal of Industrial Ergonomics. 2007; 37(3):225–231.

[14]. Gurram R, Rakheja S, Brammer AJ. Driving-point mechanical impedance of the human hand–arm system: synthesis and model development. Journal of Sound and Vibration. 1995; 180:437–458.

[15]. ISO-10068: Mechanical Vibration and Shock—Free, Mechanical Impedance of the Human Hand—Arm System at the Driving Point. International Organization of Standard; Geneva, Switzerland: 1998.

[16]. Wu JZ, Dong RG, Welcome DE, Xu XS. A method for analyzing vibration power absorption density in human fingertip. Journal of Sound and Vibration. 2010; 329:5600–5614.

[17]. Dong RG, Rakheja S, Schopper AW, Han B, Smutz WP. Hand-transmitted vibration and biodynamic response of the human hand–arm: a critical review. Critical Reviews™ in Biomedical Engineering. 2001; 29(4):391–441.

[18]. Rakheja S, Wu JZ, Dong RG, Schopper AW. A comparison of biodynamic models of the human hand–arm system for applications to hand-held power tools. Journal of Sound and Vibration. 2002; 249(1):55–82.

[19]. Dong RG, Welcome DE, Wu JZ, McDowell TW. Development of hand–arm system models for vibrating tool analysis and test rig construction. Noise Control Engineering Journal. 2008; 56(1): 35–44.

[20]. Dong, RG.; McDowell, TW.; Welcome, DE.; Wu, JZ.; Warren, C.; Smutz, WP.; Schopper, AW. Mechanical energy absorption in human fingers exposed to hand-transmitted vibration. In: Vossoughi, J., editor. Biomedical Engineering: Recent Developments. Medical and Engineering Publishers, Inc; 2002. p. 159-160.

[21]. Dong RG, Wu JZ, McDowell TW, Welcome DE, Schopper AW. Distribution of mechanical impedance at the fingers and the palm of human hand. Journal of Biomechanics. 2005; 38(5): 1165–1175. [PubMed: 15797597]

[22]. Dong RG, Dong JH, Wu JZ, Rakheja S. Modeling of biodynamic responses distributed at the fingers and the palm of the human hand–arm system. Journal of Biomechanics. 2007; 40:2335–2340. [PubMed: 17166500]

[23]. Dong JH, Dong RG, Rakheja S, Welcome DE, McDowell TW, Wu JZ. A method for analyzing absorbed power distribution in the hand and arm substructures when operating vibrating tools. Journal of Sound and Vibration. 2008; 311:1286–1309.

[24]. Dong RG, McDowell TW, Welcome DE, Warren C, Wu JZ, Rakheja S. Analysis of anti-vibration gloves mechanism and evaluation methods. Journal of Sound and Vibration. 2009; 321:435–453.

[25]. ISO-10068/DIS: Mechanical Vibration and Shock—Free. Mechanical Impedance of the Human Hand–Arm System at the Driving Point. International Organization of Standard; Geneva, Switzerland: 2012.

[26]. Adewusi S, Rakheja S, Marcotte P. Biomechanical models of the human hand–arm to simulate distributed biodynamic responses for different postures. International journal of Industrial Ergonomics. 2012; 42:249–260.

[27]. Dong RG, Welcome DE, Xu XS, Warren C, McDowell TW, Wu JZ, Rakheja S. Mechanical impedances distributed at the fingers and palm of the hand–arm system in three orthogonal directions. Journal of Sound and Vibration. 2012; 331:1191–1206.

[28]. ISO 10819: Mechanical Vibration and Shock—Hand-Arm Vibration. International Organization for Standardization; Geneva, Switzerland: 1996. Method for the Measurement and Evaluation of the Vibration Transmissibility of Gloves at the Palm of the Hand.

[29]. Welcome DE, Dong RG, Xu XS, Warren C, McDowell TW, Wu JZ. An investigation on the 3-D vibration transmissibility on the human hand–arm system using a 3-D scanning laser vibrometer. Canadian Acoustics. 2011; 39(2):44–45.

[30]. Dong RG, Welcome DE, McDowell TW, Wu JZ. Methods for deriving representative biodynamic response of hand–arm system to vibration. Journal of Sound and Vibration. 2009; 325:1047–1061.

[31]. McDowell, TW.; Welcome, DE.; Xu, XS.; Warren, C.; Dong, RG. Proceedings of the Fourth American Conference on Human Vibration. Hartford, CT, USA: 2012. The transmissibility of vibration-reducing gloves at the palm of the hand in three orthogonal directions; p. 6-7.

[32]. Welcome, DE.; Dong, RG.; Xu, XS.; Warren, C.; McDowell, TW.; Wu, JZ. Proceedings of the Fourth American Conference on Human Vibration. Hartford, CT, USA: 2012. Effectiveness of anti-vibration gloves for reducing finger vibration; p. 6-7.

[33]. Griffin MJ. Measurement, evaluation, and assessment of occupational exposures to hand-transmitted vibration. Occupational Environmental Medicine. 1997; 54:73–89. [PubMed: 9072014]

[34]. Dong RG, Rakheja S, McDowell TW, Welcome DE, Wu JZ. Estimation of the biodynamic responses distributed at fingers and palm based on the total response of the hand–arm system. International Journal of Industrial Ergonomics. 2010; 40(4):425–436.

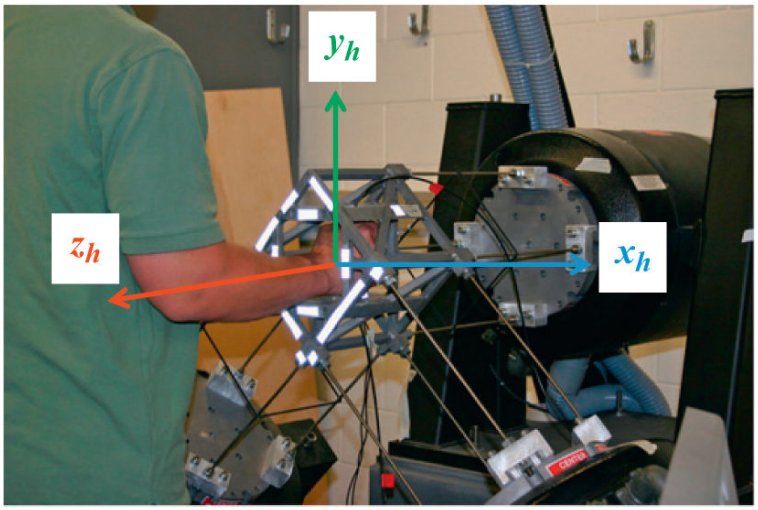

Fig. 1.

A pictorial view of the test setup and subject postures for the measurements of the driving-point mechanical impedances and vibration transmissibility of the hand–arm system in the three orthogonal directions on a 3-D hand–arm vibration test system [27,29].

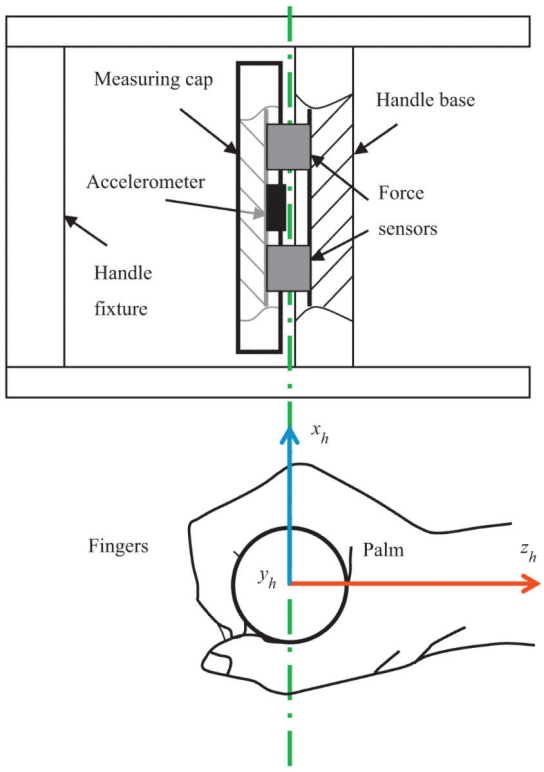

Fig. 2.

A sketch of the 3-D instrumented handle and hand grip posture used in the measurement of the mechanical impedances distributed at the fingers and palm of the hand in the three orthogonal directions [27].

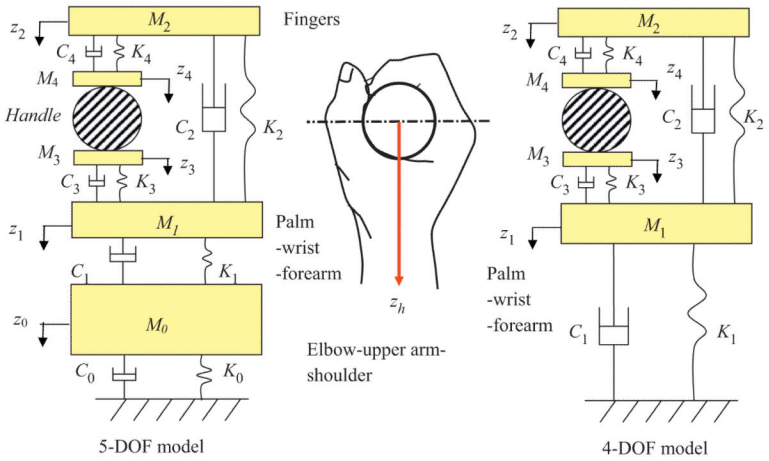

Fig. 3.

Hand grip posture and the configurations of the two models of the hand–arm system along the forearm, or z_h direction.

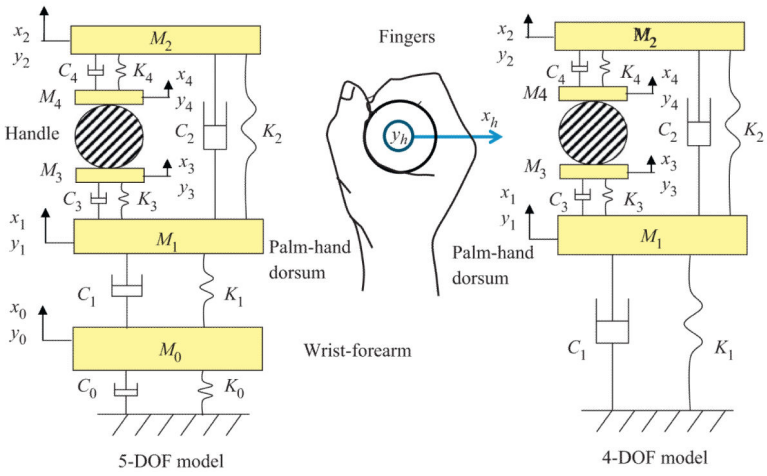

Fig. 4.

Hand grip posture and the configurations of the two models of the hand–arm system for the x_h and y_h directions.

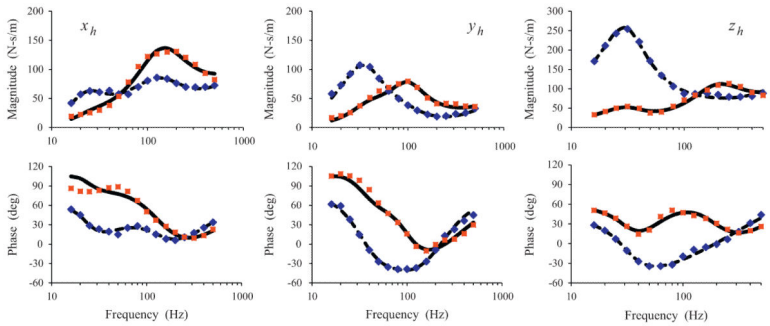

Fig. 5.

Comparisons of the experimental data and the 5-DOF modeling results of the driving-point mechanical impedances distributed at the fingers and palm of the hand in the three orthogonal directions (■, experiment_fingers; —, modeling_fingers; ◆, experiment_palm; ——, modeling palm).

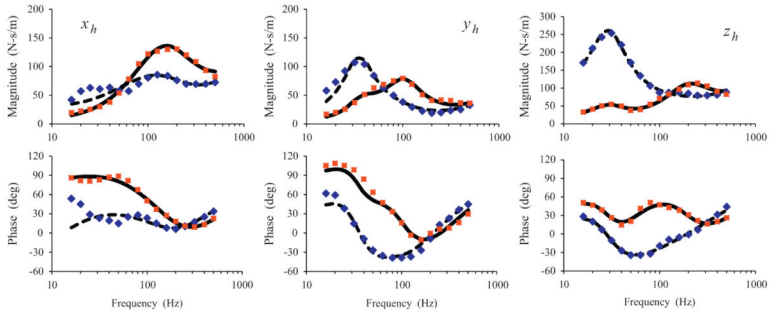

Fig. 6.

Comparisons of the experimental data and the 4-DOF modeling results of the driving-point mechanical impedances distributed at the fingers and palm of the hand in the three orthogonal directions (■, experiment_fingers; —, modeling_fingers;, ◆, experiment_palm; ——, modeling_palm).

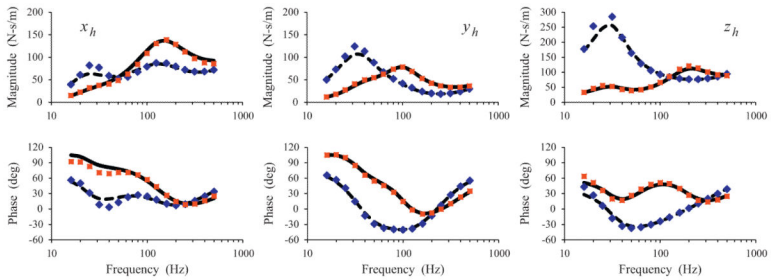

Fig. 7.

Comparisons of the driving-point mechanical impedances predicted using the 5-DOF models established based on the mean response-based and mean property-based approaches (◆, fingers_property-based approach; —, fingers_response-based approach; ■, palm_property-based approach; ——, palm_response-based approach).

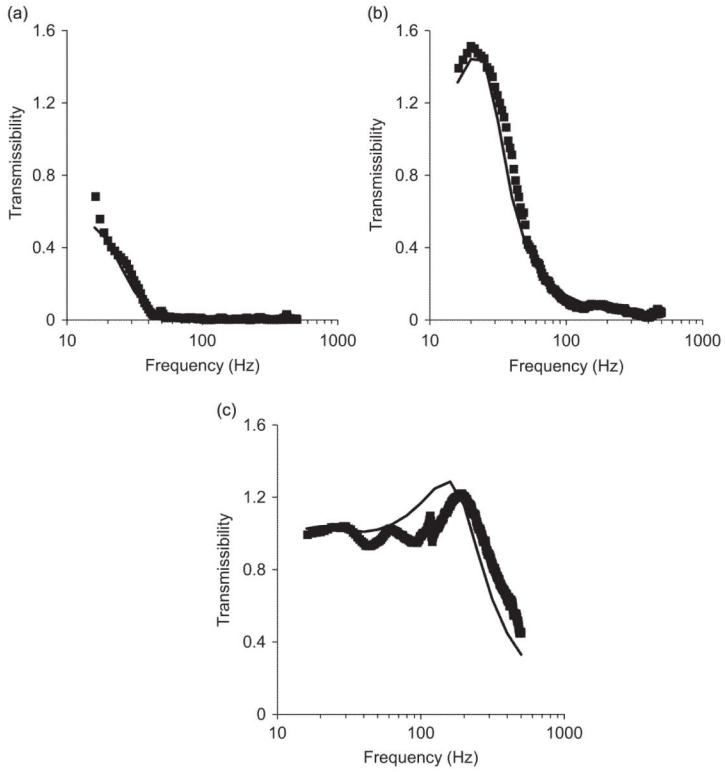

Fig. 8.

Comparisons of the model-predicted and measured vibration transmissibility magnitudes in the z_h direction at three locations: (a) upper arm; (b) wrist; and (c) fingers (—, predicted; ■■■, measured [29]).

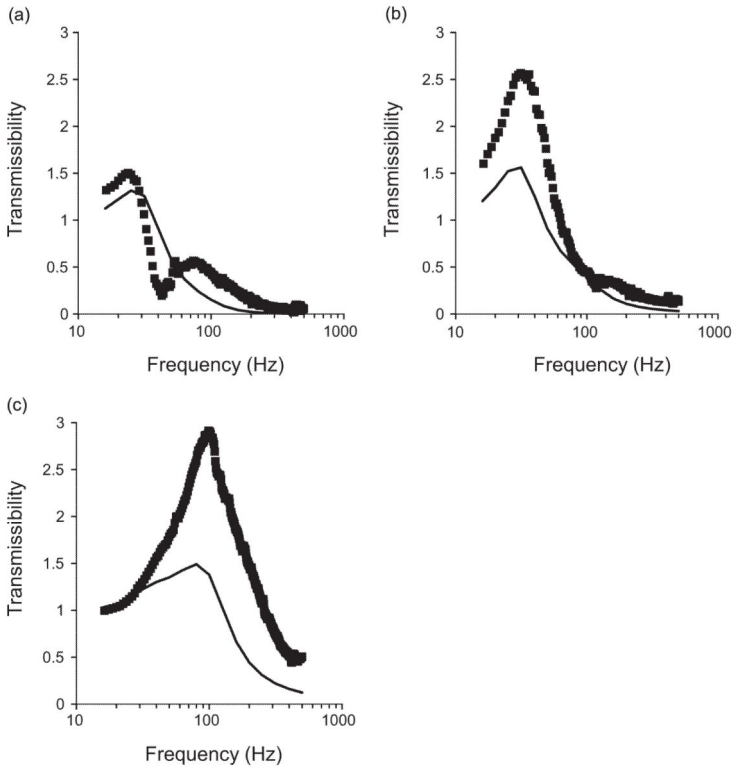

Fig. 9.

Comparisons of the model-predicted and measured vibration transmissibility magnitudes in the y_h direction at three locations: (a) wrist; (b) hand dorsum; and (c) fingers (—, predicted; ■■■, measured [29]).

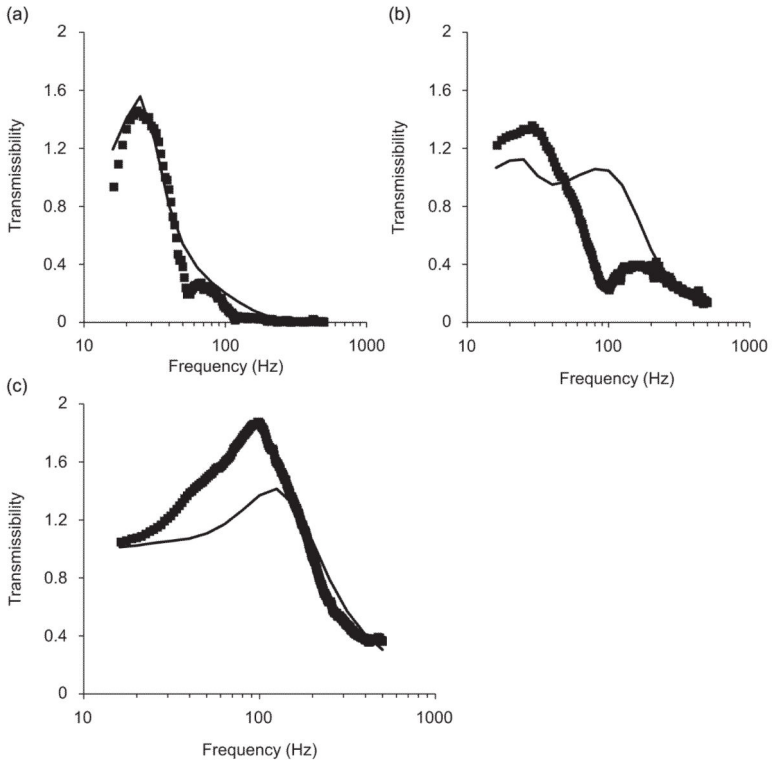

Fig. 10.

Comparisons of the model-predicted and measured vibration transmissibility magnitudes in the x_h direction at three locations: (a) wrist; (b) hand dorsum; and (c) fingers (—, predicted; ■■■, measured [29]).

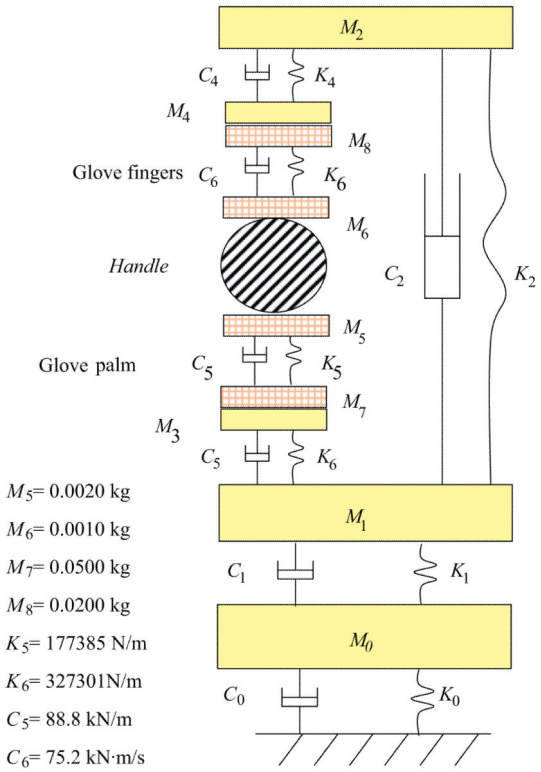

Fig. 11.

The model of the glove-hand-arm system and the parameters of the glove model included in a proposed revision of ISO 10068 [25].

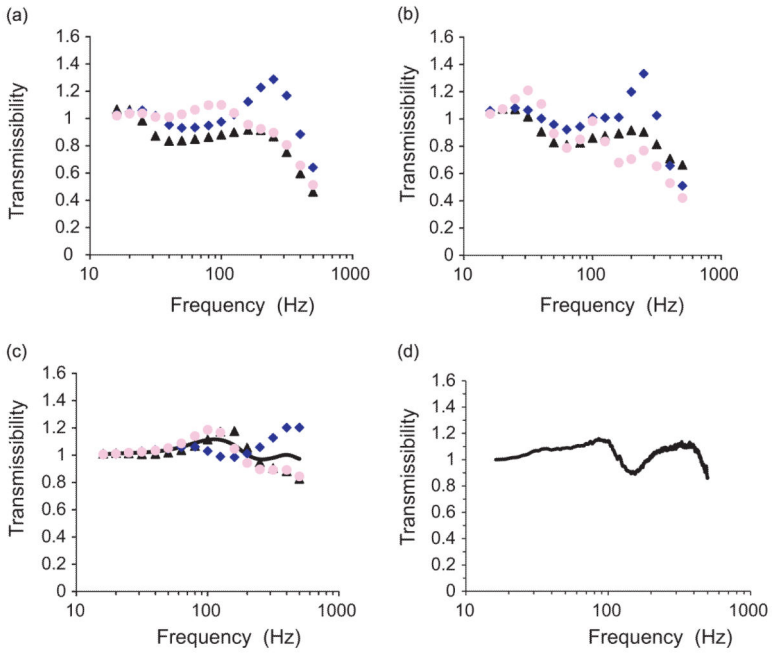

Fig. 12.

Comparisons of the model-predicted and measured glove transmissibility functions: (a) modeling_palm; (b) experiment palm [31]; (c) experiment_fingers [32]; (d) modeling_fingers (●, x_h direction; ◆, y_h direction; ▲, z_h direction; —, total vibration).

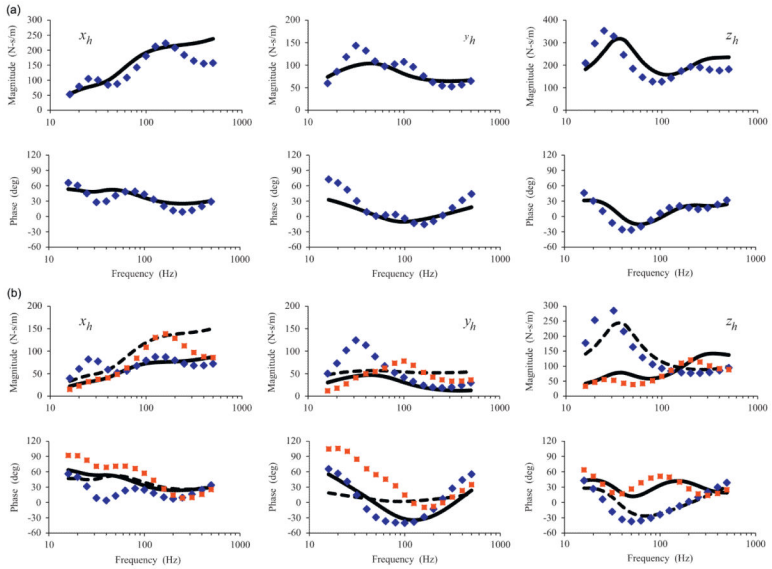

Fig. 13.

Comparisons of the mechanical impedances predicted using the new models developed in the current study and those included in the proposed revision of ISO 10068 [25] in the three orthogonal directions: (a) the impedances of the entire hand-arm system (—, proposed ISO model; ◆, new model); (b) the impedances distributed at the fingers and palm of the hand (■, new model_fingers; —, proposed ISO model_fingers; ◆, new model_palm; ——, proposed ISO model_palm).

Table 1

Parameters of the response-based models in the three orthogonal directions (x_h, y_h, and z_h) determined from the arithmetic means of the subject experimental data [27].

ID	Unit	x_h direction		y_h direction		z_h direction	
		5-DOF	4-DOF	5-DOF	4-DOF	5-DOF	4-DOF
M_0	kg	0.300		0.300		4.000	
M_1	kg	0.188	0.222	0.250	0.388	1.263	1.281
M_2	kg	0.079	0.075	0.079	0.079	0.075	0.074
M_3	kg	0.015	0.016	0.009	0.009	0.022	0.022
M_4	kg	0.014	0.015	0.009	0.009	0.015	0.015
K_0	N/m	1152		1000		20,357	
K_1	N/m	5648	1000	1000	1000	5442	1000
K_2	N/m	10	10	10	10	5699	5492
K_3	N/m	41,749	38,484	19,354	17,064	37,714	36,861
K_4	N/m	114,031	124,102	32,881	34,113	10,0159	102,050
C_0	N s/m	10.2		5.0		169.3	
C_1	N s/m	36.2	34.4	43.7	18.8	117.7	110.7
C_2	N s/m	67.2	64.4	16.4	16.7	25.4	25.9
C_3	N s/m	55.9	57.5	17.3	22.3	72.6	73.6
C_4	N s/m	76.0	72.2	28.7	27.8	71.8	70.6
f_0 [a]	Hz	22.6		12.8		12.6	
f_1 [a]	Hz	80.3	67.2	45.4	34.4	31.3	29.4
f_2 [a]	Hz	191.2	204.3	102.7	92.6	188.8	191.9

[a] f_0, f_1 and f_2 are undamped natural frequencies of model.

Table 2

Comparisons of the mean property-based and mean response-based 5-DOF models in the three orthogonal directions (x_h, y_h, and z_h).

ID	Unit	x_h direction		y_h direction		z_h direction	
		Response	Property	Response	Property	Response	Property
M_0	kg	0.300	0.344	0.300	0.353	4.000	4.292
M_1	kg	0.188	0.178	0.250	0.192	1.263	1.508
M_2	kg	0.079	0.081	0.079	0.079	0.075	0.078
M_3	kg	0.015	0.015	0.009	0.010	0.022	0.022
M_4	kg	0.014	0.016	0.009	0.009	0.015	0.015
K_0	N/m	1152	1611	1000	1075	20,357	38,341
K_1	N/m	5648	9988	1000	1000	5442	5168
K_2	N/m	10	3991	10	112	5699	4999
K_3	N/m	41,749	43,205	19,354	21,782	37,714	35,895
K_4	N/m	114,031	109,271	32,881	32,929	100,159	103,308
C_0	N-s/m	10.2	12.8	5.0	5.8	169.3	181.2
C_1	N s/m	36.2	36.0	43.7	91.6	117.7	93.6
C_2	N s/m	67.2	56.2	16.4	18.9	25.4	23.4
C_3	N s/m	55.9	57.0	17.3	16.7	72.6	73.6
C_4	N s/m	76.0	65.8	28.7	27.8	71.8	68.7
f_0 [a]	Hz	22.6	26.7	12.8	12.1	12.6	15.9
f_1 [a]	Hz	80.3	90.9	45.4	54.9	31.3	27.8
f_2 [a]	Hz	191.2	188.5	102.7	102.7	188.8	187.3

[a] f_0, f_1 and f_2 are undamped natural frequencies of model.

Table 3

Comparisons of the proposed ISO 5-DOF models [25] and the mean property-based 5-DOF models in the three orthogonal directions (x_h, y_h, and z_h).

ID	Unit	x_h direction		y_h direction		z_h direction	
		ISO	**New**	**ISO**	**New**	**ISO**	**New**
M_0	kg	**0.2360**	0.344	**0.3605**	0.353	**7.5000**	4.292
M_1	kg	**0.3998**	0.178	**0.5515**	0.192	**1.0721**	1.508
M_2	kg	**0.0576**	0.081	**0.0725**	0.079	**0.0760**	0.078
M_3	kg	**0.0205**	0.015	**0.0050**	0.010	**0.0200**	0.022
M_4	kg	**0.0100**	0.016	**0.0030**	0.009	**0.0100**	0.015
K_0	N/m	**1000**	1611	**1000**	1075	**8059**	38,341
K_1	N/m	**6972**	9988	**1000**	1000	**1891**	5168
K_2	N/m	**100**	3991	**100**	112	**12,000**	4999
K_3	N/m	**4000**	43,205	**5443**	21,782	**44,220**	35,895
K_4	N/m	**65,844**	109,271	**15,170**	32,929	**176,880**	103,308
C_0	N s/m	**21.8**	12.8	**40.5**	5.8	**93.1**	181.2
C_1	N s/m	**22.1**	36.0	**95.7**	91.6	**112.1**	93.6
C_2	N s/m	**69.8**	56.2	**37.6**	18.9	**39.7**	23.4
C_3	N s/m	**128.6**	57.0	**51.5**	16.7	**83.9**	73.6
C_4	N s/m	**81.5**	65.8	**11.4**	27.8	**116.7**	68.7
f_0 [a]	Hz	22.6	26.7	12.8	12.1	12.6	15.9
f_1 [a]	Hz	80.3	90.9	45.4	54.9	31.3	27.8
f_2 [a]	Hz	191.2	188.5	102.7	102.7	188.8	187.3

[a] f_0, f_1 and f_2 are undamped natural frequencies of model.